Aginaga, J.; Iriarte Goñi, X.; Plaza, A.; Mata Amela, V. (2018). Kinematic Design of a New Four Degree-of-Freedom Parallel Robot for Knee Rehabilitation. Journal of Mechanical Design. 140(9). https://doi.org/10.1115/1.4040168

Jokin Aginaga[1]
Institute of Smart Cities (ISC),
Public University of Navarre,
Iruñea-Pamplona 31006, Spain
e-mail: jokin.aginaga@unavarra.es

Xabier Iriarte
Institute of Smart Cities (ISC),
Public University of Navarre,
Iruñea-Pamplona 31006, Spain
e-mail: xabier.iriarte@unavarra.es

Aitor Plaza
Department of Mechanical,
Energetics and Materials Engineering,
Public University of Navarre,
Iruñea-Pamplona 31006, Spain
e-mail: aitor.plaza@unavarra.es

Vicente Mata
Professor
Centro de Investigación en Ingeniería Mecánica,
Universitat Politècnica de València,
Valencia 46022, Spain
e-mail: vmata@mcm.upv.es

Kinematic Design of a New Four Degree-of-Freedom Parallel Robot for Knee Rehabilitation

Rehabilitation robots are increasingly being developed in order to be used by injured people to perform exercise and training. As these exercises do not need wide range movements, some parallel robots with lower mobility architecture can be an ideal solution for this purpose. This paper presents the design of a new four degree-of-freedom (DOF) parallel robot for knee rehabilitation. The required four DOFs are two translations in a vertical plane and two rotations, one of them around an axis perpendicular to the vertical plane and the other one with respect to a vector normal to the instantaneous orientation of the mobile platform. These four DOFs are reached by means of two RPRR limbs and two UPS limbs linked to an articulated mobile platform with an internal DOF. Kinematics of the new mechanism are solved and the direct Jacobian is calculated. A singularity analysis is carried out and the gained DOFs of the direct singularities are calculated. Some of the singularities can be avoided by selecting suitable values of the geometric parameters of the robot. Moreover, among the found singularities, one of them can be used in order to fold up the mechanism for its transportation. It is concluded that the proposed mechanism reaches the desired output movements in order to carry out rehabilitation maneuvers in a singularity-free portion of its workspace. [DOI: 10.1115/1.4040168]

1 Introduction

Parallel manipulators (PMs) have focused the interest of many researchers and industries due to their advantages compared to serial robots. Since their end-effector is sustained by several kinematic chains, they can achieve better structural and dynamic properties with less structural mass [1]. Lower-mobility parallel manipulators are those having less than 6DOFs. Their main advantages are a simpler architecture and lower cost of design and manufacturing. They have been used in many applications such as machine tool [2–4], pick-and-place operations [5–9], and medical (surgical or rehabilitation) robots [10–13]. For each application or required task, the designed parallel robot has the corresponding number and type of translational or rotational DOFs.

Focusing on the rehabilitation of the lower limb, most of the parallel manipulators developed until now have two or three rotational degrees-of-freedom (DOFs), mainly because they focus on ankle rehabilitation [14]. Those proposals can be suitable for very restricted motions such as the one which takes place in ankle rehabilitation. However, they cannot be extended to rehabilitation of other human joints such as the knee or hip. These joints require large flexion–extension motion in the tibiofemoral plane (the plane that form the tibia and the femur) as well as small rotations involving systems with three or more DOFs of which at least two must be translational motions. Obviously, a 6DOF parallel manipulator could be used for this purpose [15]; however, this solution increases the cost and complicates the dynamic robot control [14].

This work deals with the design of a new parallel manipulator to be used for knee rehabilitation. The main goal is to assist to the rehabilitation of the anterior cruciate ligaments (ACLs) after surgery. Figure 1 shows the ACL together with other parts of the knee.

The foot of the injured leg will be located in a mobile platform which imposes rehabilitation movements to it. In terms of rehabilitation requirements, the knee joint can rotate around the transverse (with regard to the tibiofemoral plane) axis and the vertical (with regard to the mobile platform) axis. Moreover, the knee could be translated in the tibiofemoral plane. It is also intended that the proposed design for the parallel manipulator be able to perform diagnostic tests on the condition of the ACL.

Nowadays, there are two tests that are currently used to diagnose ACL injuries: the Lachman test [16] and the Pivot Shift test [17]. The Lachman test assesses ACL tear by displacing the tibia relative to the femur. To reproduce the Lachman test, the PM requires two perpendicular translations in the tibiofemoral plane and a rotation perpendicular to it. The pivot shift test is intended to reproduce translational and rotational instability in the knee by applying a twist to the tibia and essentially measuring the rotation. To reproduce the pivot shift test, the robot should provide a rotation about an axis contained in the tibiofemoral plane.

The range of motion needed has been established according to the values for major rotations in the joints of the ankle, knee, and hip determined in Ref. [18], and considering also the specific characteristics of the diagnosis mentioned above. Based on this, the novel PM should perform the following basic movements shown in Fig. 2:

(1) Flexion of the limb in the direction perpendicular to the tibiofemoral plane. The total range must be at least 60 deg for rehabilitation purposes.
(2) Rotation of the limb along an axis perpendicular to the mobile platform. The range of motion must be at least ±10 deg (Pivot Shift).
(3) Translation in the direction of a horizontal axis contained in the tibiofemoral plane. The displacement is small, 15–20 mm, in order to reproduce the Pivot Shift or Lachman tests. However, in order to perform some of the movements planned for rehabilitation, this horizontal displacement should be increased to a total of at least 400 mm.
(4) Translation in the direction of a vertical axis contained in the tibiofemoral plane. Major shifts may be required, at least 200 mm, in coordination with the horizontal movement previously described to reproduce rehabilitation

[1]Corresponding author.

Contributed by the Mechanisms and Robotics Committee of ASME for publication in the Journal of Mechanical Design. Manuscript received July 31, 2017; final manuscript received April 18, 2018; published online July 3, 2018. Assoc. Editor: Oscar Altuzarra.

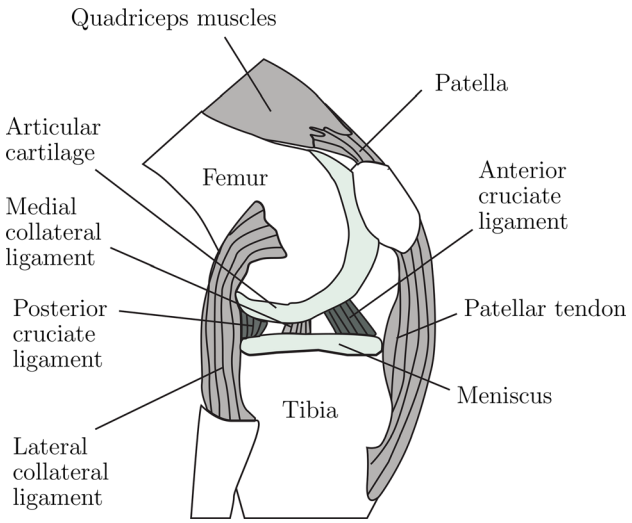

Fig. 1 Illustration of the knee ligaments and bones

motions. Also, from a practical point of view, a greater displacement was required in order to properly locate the mobile platform where the patients foot rests.

Another requirement is a compact design in order to be translated from one room to another in a hospital or even to the patient's home. In order to achieve this requirement, the proposed mechanism must have the ability to fold up or to be carried to a configuration in which it takes the minimum possible volume.

An overview of the literature shows that there exist several two translation and two rotation (2T2R) robots but the output DOFs do not coincide with the ones required for knee rehabilitation. Specifically, rotations of most 2T2R robots in the literature are with respect to axes contained in the plane of the mobile platform. In Ref. [19], a 2T2R parallel manipulator is presented and used for the construction of a five-axis parallel machine tool. More recently, Ref. [20] develops a systematic synthesis of some 2T2R and other mechanisms and suggests some applications for

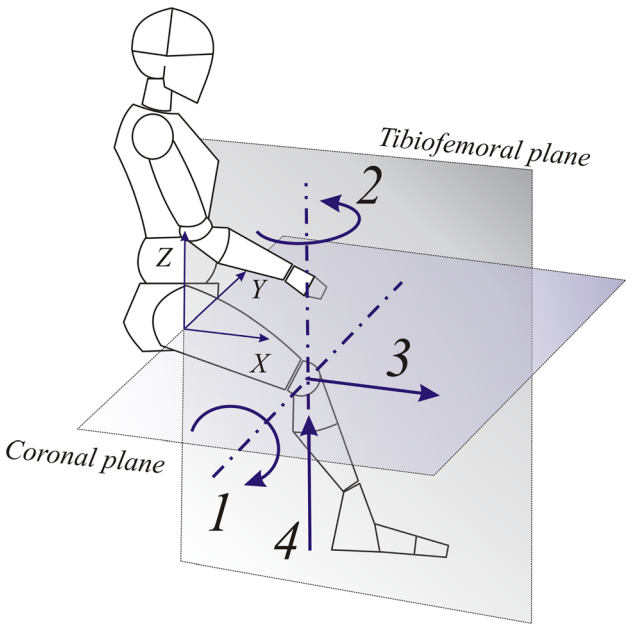

Fig. 2 Movements of the required rehabilitation task

synthesized mechanisms such as machine tool or damping devices. An additional 2T2R parallel mechanism is shown in Ref. [21] for turbine blade machining, which has some partially decoupled DOFs. Altuzarra et al. [22] introduce another 2T2R parallel mechanism, which is used as a solar tracker and designed with the aim of minimizing the energy consumption during its operation. One more 2T2R PM is presented in Ref. [23], whose design is optimized for its application in automated fiber placement for aerospace part manufacturing.

Moreover, the synthesis of some other 2T2R parallel mechanisms is introduced in Ref. [24], which is designed as medical robots for the task of needle manipulation. A task-based synthesis procedure is used using a remote center of motion point as a key requirement for the synthesized mechanisms.

None of the mechanisms cited so far can be applied to the required knee rehabilitation task, since they have their rotations DOFs with respect to axes located in the mobile platform instead of having a rotation around an axis perpendicular to it. In some cases, this fact could be corrected changing the orientation of some of the aforementioned robots, placing their fixed platform in vertical and designing an appropriate mobile platform. Nevertheless, the resulting robot would be a cantilever mechanism suffering high bending loads. A planar mechanism moving in a vertical plane could avoid such bending loads and such an arrangement is presented in Ref. [25], but it has only three DOFs lacking the rotation perpendicular to the mobile platform, which is necessary to cruciate ligament rehabilitation.

To the best of our knowledge, only two references show mechanisms that could be usable for the required rehabilitation task according to their kinematics. The first one presents a type synthesis procedure for multiloop mechanisms [26]. Among the synthesized mechanisms, there are some 2R2T mechanisms which could have the desired output DOFs, but the use of curved bars in order to obtain intersecting joint axes could lead to a lack of stiffness which is not desired for the knee rehabilitation application. The second one presents 2R3T and 2R2T parallel mechanisms using articulated mobile platforms [27]. Two of the presented architectures can perform the required output DOFs. Nevertheless, the former has a topology similar to the Delta robot with rotational actuators and parts subject to bending loads that make the stiffness performance worse. Thus, it seems to be applicable for fast, light tasks such as pick-and-place operations. The latter, in turn, has a structure with fixed prismatic actuators which allows a better stiffness performance, but it prevents achieving a compact configuration in which the mechanism can be easily translated.

Besides the already cited mechanisms, in Refs. [28] and [29], a mechanism accomplishing the required DOFs, but with a very different topology, is presented, which has been developed in parallel to the one presented here in the environment of the same research projects. A comparison study between this mechanism and the one presented here will determine which of them is better for the required rehabilitation tasks.

This work presents a new architecture of a 2T2R parallel mechanism with a 2RPRR-2 UPS topology for knee rehabilitation and its kinematic analysis. In order to allow the required DOFs, it uses an articulated mobile platform instead of a rigid one. Further, a rigid platform is located on the articulated platform, since a rigid body is required in order to put the patients foot on it. Articulated platforms have been proposed to perform the rotation in 3T1R fast parallel robots [30] or to be used as a gripper, instead of a gripper in series to the end-effector, reducing the inertia of the robot [31–33]. In this case, the articulated mobile platform is used to allow the mechanism to have a high rotational capability, as in Ref. [27], specially required for the rotation perpendicular to the tibiofemoral plane. The designed mechanism also fulfills the requirements of having a compact configuration in which it can be translated. In addition, it uses prismatic actuators to reduce bending loads in order to be stiffer.

The paper is organized as follows: Sec. 2 describes the architecture of the 2RPRR-2 UPS mechanism and shows a preliminary

CAD design. Kinematics equations are written and solved in Sec. 3, together with the calculation of the Jacobian matrix. A singularity analysis is carried out in Sec. 4 and the null space of the listed singularities is also calculated. Section 5 shows the location of the singularities within the workspace and presents a rehabilitation maneuver. Finally, in Sec. 6, some conclusions are addressed.

2 The 2RPRR-2 UPS Mechanism

The 2RPRR-2 UPS mechanism has two identical RPRR limbs, $i = 1, 3$, and two UPS limbs, $i = 2, 4$. The fixed base is a square and the articulated mobile platform is a planar four-bar mechanism with the same length for the four bars. Figure 3 shows its schematic representation.

In the RPRR limbs, the axis of the first revolute joint at A_1 and A_3 is horizontal in the y direction. Consequently, the actuated prismatic joint is contained in a vertical plane. Next, R joint is located at points B_1 and B_3 and oriented as the first one, with its axis in the y direction. Finally, the axis of the last R joint is perpendicular to the previous R joint and to the mobile platform. This last R joint connects the RPRR limb to a bar of the four-bar mechanism at C_1 and C_3. On the other hand, the UPS limbs have a first universal joint with its first-fixed axis horizontal in the x direction and the second one perpendicular to the first one and to the prismatic pair of the limb. These universal joints are located at points A_2 and A_4. The actuated prismatic joints connect the fixed base with a bar of the four-bar mechanism that forms the mobile platform by means of spherical joints located at C_2 and C_4. The reference point P of the mobile platform is located at the geometric center of the articulated mobile platform. A frame u-v-w is located in the mobile platform in such a way that **u** vector points from P to C_1 and **w** vector is perpendicular to the plane containing the four-bar mechanism. Notice that **w** vector will always be contained in a vertical plane.

With such a topology, points C_1 and C_3 belong to vertical planes and, since the bars of the four-bar mechanism are equal, they constrain its center—the reference point P—to be in the vertical x-z plane. As a consequence, there will not be parasitic translations of the platform in the y direction. In turn, R joints at B_1 and B_3 allow the plane of the four-bar mechanism to rotate with respect to the y axis. Finally, the internal DOF of the mobile platform allows the rotation of u with respect to w, and thus, the second rotation of the mobile platform. Hence, the 4DOFs of the mobile platform are displacement in x and z of point P and rotations of the mobile platform about the y and w directions, namely, those desired for the rehabilitation exercises. Since the axes of the first two R joints of the RPRR limb are parallel to each other and perpendicular to the x-z plane, the axis of the last R joint is contained in x-z. This fact makes that the plane in which the articulated mobile platform is contained can only rotate about the y axis. Hence, there is no parasitic rotation and the reference u-v-w can only rotate about two axes, namely y and w.

In the schematic view of the mechanism shown in Fig. 3, it can be noticed that there is no physical mobile platform, with point P being a virtual point at the center of the parallelogram formed by bars C_iC_j. In order to design a physical mobile platform, a system of linear bearings is used. This system consists of two perpendicular guides, one from C_1 to C_3 and another from C_2 to C_4, and four carriages or linear bearings, each of them attached to one of the C_i points. Figure 4 shows the way the guides are located at the bottom of the mobile platform together with the carriages of the linear bearings.

With the design shown in Fig. 4, a rigid mobile platform can be placed on the four-bar linkage. Notice that the center of the mobile platform will always coincide with the center of the parallelogram. This rigid mobile platform allows the foot of the patient to be located on it. A preliminary CAD design of the complete mechanism is shown in Fig. 5, with and without the mobile platform.

For the described joints of the mechanism without the mobile platform, the mechanism is over-constrained with four redundant constraints. Since it has a planar articulated four-bar mechanism with parallel R joints, replacing two of them with U and S joints would remove three of its redundant constraints. The last one could be removed by replacing the R joint at B_1 or B_3 with a cylindrical C joint.

An attempt to show that the mechanism reaches the four output DOFs required in rehabilitation tasks is shown in Fig. 6. The movement of each of the four output DOFs is represented, while the other DOFs remain constant. In order to show it clearly, the starting configuration is same in four figures and the second configuration is presented with dotted lines.

2.1 Other Possible Architectures. The design presented is not the only solution for creating the desired 2T2R output DOFs. Using the same passive and actuated joints, a 2PRRR-2PUS architecture could also be a solution. Nevertheless, the volume of the mechanism with fixed prismatic actuators is larger at any configuration and this fact complicates the translation of the mechanisms from one place to another (for example, from one room to another in a hospital or even to a patient's home). From such point of view, the chosen 2RPRR-2 UPS architecture is more compact by taking the manipulator to the singularity shown later in Sec. 4.

Another design option could be the one with revolution actuators instead of prismatic ones, having a 2RRRR-2RUS architecture. This change leads to an architecture similar to one 2T2R mechanism shown in Ref. [27], which produces the same required output DOFs. As said before, the resulting mechanisms should be more suitable for fast, light tasks such as pick-and-place operations, since they seem to be too weak to support the mass of a human leg.

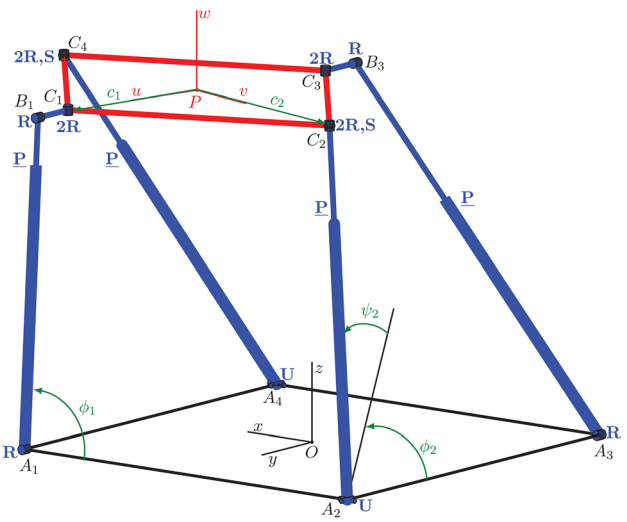

Fig. 3 Schematic model of the 2-RPRR-2 UPS mechanism

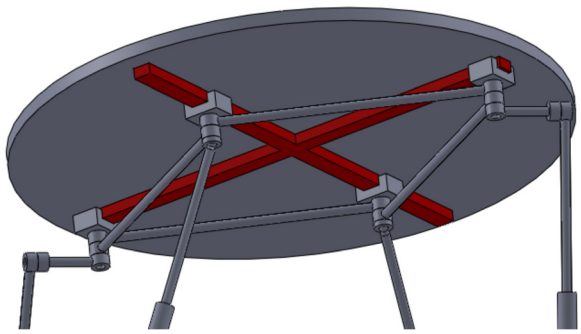

Fig. 4 View of the guides at the mobile platform

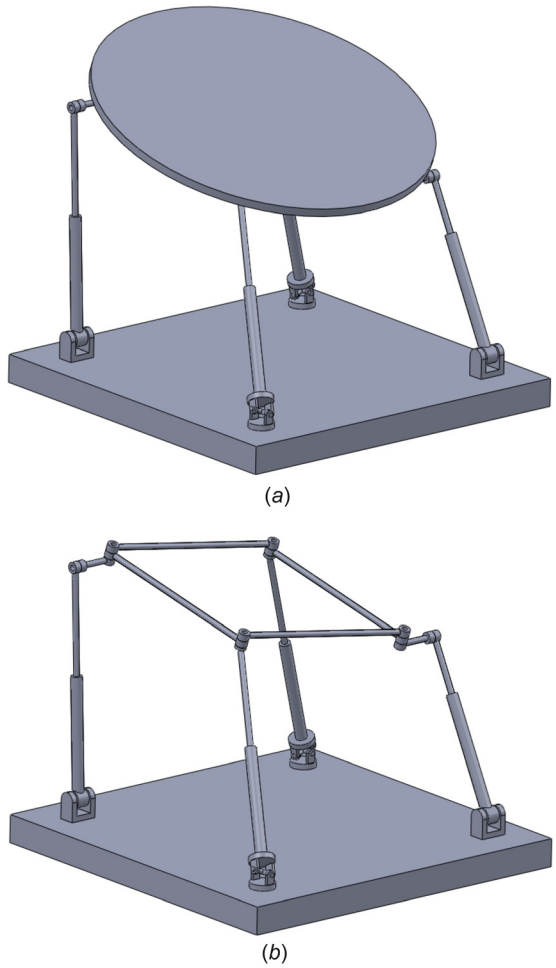

Fig. 5 Preliminary CAD model of the mechanism: (*a*) with mobile platform and (*b*) without mobile platform

3 Kinematics of the 2RPRR-2 UPS Mechanism

First, geometric parameters L, e, and r of the mechanism are defined. Figure 7 shows a top view of the mechanism with its mobile platform horizontal showing the said parameters:

L: length of the side of the square fixed platform e: length of B_iC_i bars ($i=1,\ 3$) r: length of the bars of the mobile parallelogram

Kinematics are solved using 16 coordinates. The inputs of the mechanism are the prismatic actuators from A_i to B_i ($i=1,\ 3$) or C_i ($i=2,\ 4$), whose lengths are described by ρ_i coordinates. On the other hand, the outputs are the Cartesian coordinates x_P and z_P of point P and Euler angles φ with respect to the fixed y-axis and γ with respect to the mobile w-axis (see Fig. 3).

Passive coordinates used to solve the kinematic problem are angles ϕ_1 and ϕ_3 of R joints at points A_1 and A_3, angles ϕ_2, ψ_2, ϕ_4, and ψ_4 of U joints at points A_2 and A_4, and distances c_1 and c_2 from point P to points C_1 and C_2, respectively. In order to make it clearer, coordinates ϕ_1, ϕ_2, ψ_2, c_1, and c_2 are depicted in Fig. 3.

Since the four bars of the articulated mobile platform have the same length, distances from point P to points C_3 and C_4 are equal to c_1 and c_2, respectively, and there is no need to define coordinates for them. As we will see later, the lack of additional coordinates for C_3 and C_4 avoids the superposition of points C_2 and C_4 for $c_2 \neq 0$, which prevents a bifurcation when modeling the singularity.

Taking into account that the mechanism has two types of limbs, two types of kinematic closed loop equations can be written

$$\mathbf{a}_i + \boldsymbol{\rho}_i + e(\pm\mathbf{j}) = \mathbf{p} + \mathbf{R}\,\mathbf{c}_i^{uvw} \quad i = 1,3 \tag{1}$$

$$\mathbf{a}_i + \boldsymbol{\rho}_i = \mathbf{p} + \mathbf{R}\,\mathbf{c}_i^{uvw} \quad i = 2,4 \tag{2}$$

where $\mathbf{a}_i$ stands for position vectors from the origin O to A_i, $\boldsymbol{\rho}_i$ are vectors from A_i to B_i ($i=1,\ 3$) or C_i ($i=2,\ 4$), $\mathbf{j}$ is the unit vector in the y direction, $\mathbf{p}$ is the position vector from the origin O to the reference point P of the mobile platform, $\mathbf{R}$ is the rotation matrix from u-v-w to x-y-z, and $\mathbf{c}_i^{uvw}$ are position vectors from P to C_i expressed in base u-v-w. The sign for $\pm$ in Eq. (1) is $-$ for $i=1$ and $+$ for $i=3$.

In addition to the closed loop Eqs. (1) and (2), points P, C_1, and C_2 form a right triangle so that coordinates c_1 and c_2 are related by Pythagoras Theorem

$$c_1^2 + c_2^2 = r^2 \tag{3}$$

Finally, it must be noted that the equation in the y direction in Eq. (1) is the same for both $i=1$ and $i=3$. From this equation, c_1 can be explicitly obtained as a function of γ

$$c_1 = \frac{L/2 - e}{\sin\gamma} \tag{4}$$

Then, Eqs. (1) and (2) have 11 independent equations, so that with the addition of Eq. (3), a system of 12 independent equations is obtained, which matches with the 16 coordinates and 4DOFs of the mechanism.

3.1 Inverse Kinematics. Inverse kinematics consist in solving actuator strokes ρ_i for desired output coordinates $(x_P,\ z_P,\ \varphi,\ \gamma)^T$. Solution is derived by solving $\boldsymbol{\rho}_i$ from Eqs. (1) and (2)

$$\boldsymbol{\rho}_i = \mathbf{p} + \mathbf{R}\,\mathbf{c}_i^{uvw} - \mathbf{a}_i - e(\pm\mathbf{j}) \quad i = 1,3 \tag{5}$$

$$\boldsymbol{\rho}_i = \mathbf{p} + \mathbf{R}\,\mathbf{c}_i^{uvw} - \mathbf{a}_i \quad i = 2,4 \tag{6}$$

Note that the rotation matrix $\mathbf{R}$ is known since it depends on output angles φ and γ (see Eq. (7))

$$\mathbf{R} = \begin{bmatrix} \cos\varphi\cos\gamma & -\cos\varphi\sin\gamma & \sin\varphi \\ \sin\gamma & \cos\gamma & 0 \\ -\sin\varphi\cos\gamma & \sin\varphi\sin\gamma & \cos\varphi \end{bmatrix} \tag{7}$$

In order to solve Eqs. (5) and (6), the first step is the calculation of c_1 and c_2 from Eqs. (4) and (3) respectively. Once $\mathbf{c}_i^{uvw}$ are already known, passive angles can be cancelled calculating the norm of the vectors of both sides of Eqs. (5) and (6)

$$\rho_i = \|\boldsymbol{\rho}_i\| = \|\mathbf{p} + \mathbf{R}\,\mathbf{c}_i^{uvw} - \mathbf{a}_i - e(\pm\mathbf{j})\| \quad i = 1,3 \tag{8}$$

$$\rho_i = \|\boldsymbol{\rho}_i\| = \|\mathbf{p} + \mathbf{R}\,\mathbf{c}_i^{uvw} - \mathbf{a}_i\| \quad i = 2,4 \tag{9}$$

From Eqs. (8) and (9), with the previously added information obtained from Eqs. (3) and (4), values of the actuators strokes ρ_i are obtained.

3.2 Direct Kinematics. Direct kinematics, also known as *forward kinematics*, calculates output coordinates $(x_P,\ z_P,\ \varphi,\ \gamma)^T$ for fixed strokes ρ_i of the actuators. This is a complex problem and we have not found explicit analytic expressions for the output coordinates. Although such analytic expressions would lead to a fast solution of direct kinematics problem, using an iterative numerical method for this task would not compromise the performance of a real-time application.

3.3 Jacobian and Velocity Analysis. Equations (1) and (2) can be written separated for every limb of the mechanism as

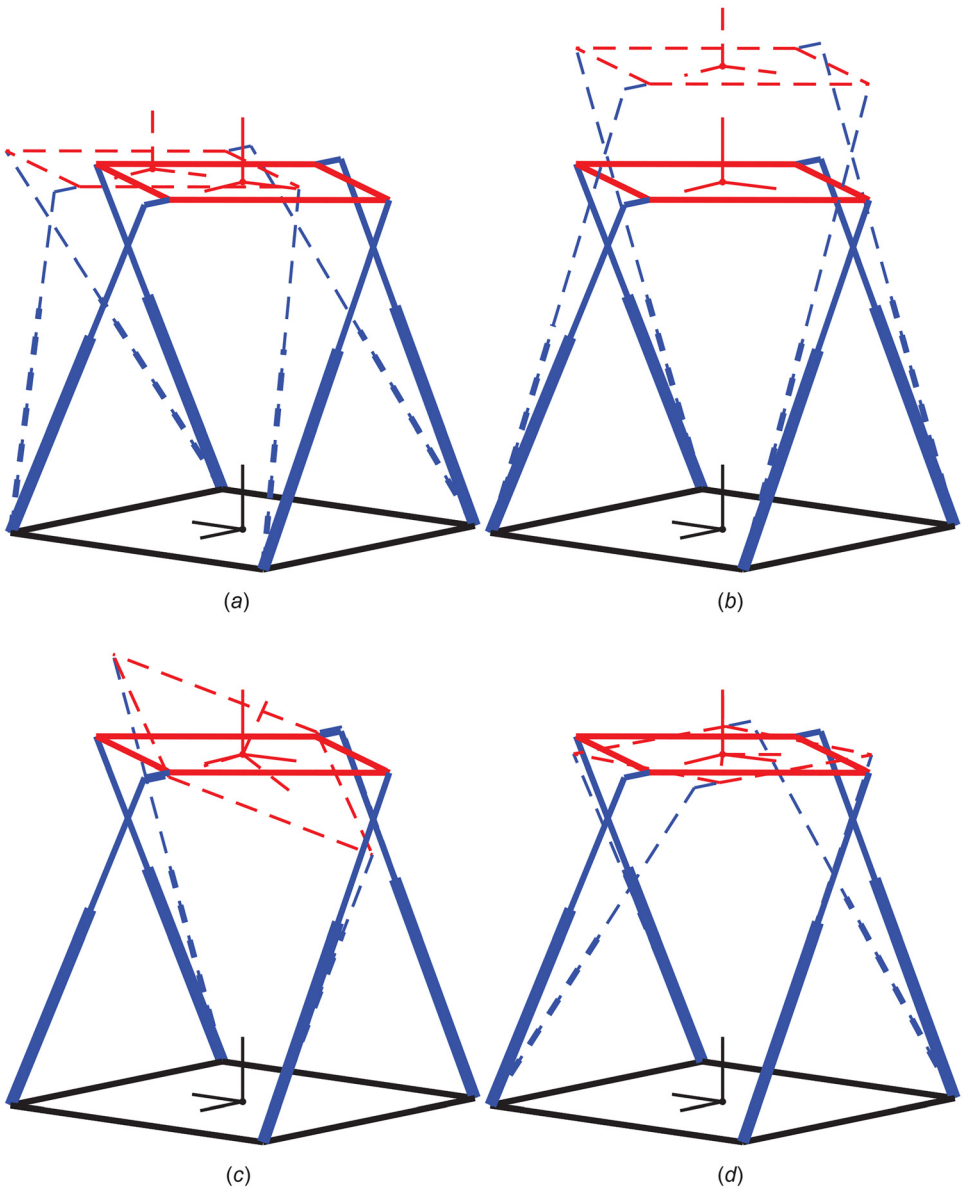

Fig. 6 Individual movements of the output DOFs: (*a*) translation in *x*, (*b*) translation in *z*, (*c*) rotation about *y*, and (*d*) rotation about *w*

$$\begin{aligned} \mathbf{a}_1 + \rho_1 \mathbf{s}_1 - e\mathbf{j} &= \mathbf{p} + c_1 \mathbf{u} \\ \mathbf{a}_2 + \rho_2 \mathbf{s}_2 &= \mathbf{p} + c_2 \mathbf{v} \\ \mathbf{a}_3 + \rho_3 \mathbf{s}_3 + e\mathbf{j} &= \mathbf{p} - c_1 \mathbf{u} \\ \mathbf{a}_4 + \rho_4 \mathbf{s}_4 &= \mathbf{p} - c_2 \mathbf{v} \end{aligned} \tag{10}$$

where $\mathbf{s}_i$ is a unit vector in the direction of the ith prismatic actuator.

Differentiating with respect to time leads to

$$\begin{aligned} \dot{\rho}_1 \mathbf{s}_1 + \rho_1 (\boldsymbol{\omega}_1 \times \mathbf{s}_1) &= \dot{\mathbf{p}} + \dot{c}_1 \mathbf{u} + c_1 (\boldsymbol{\omega}_p \times \mathbf{u}) \\ \dot{\rho}_2 \mathbf{s}_2 + \rho_2 (\boldsymbol{\omega}_2 \times \mathbf{s}_2) &= \dot{\mathbf{p}} + \dot{c}_2 \mathbf{v} + c_2 (\boldsymbol{\omega}_p \times \mathbf{v}) \\ \dot{\rho}_3 \mathbf{s}_3 + \rho_3 (\boldsymbol{\omega}_3 \times \mathbf{s}_3) &= \dot{\mathbf{p}} - \dot{c}_1 \mathbf{u} - c_1 (\boldsymbol{\omega}_p \times \mathbf{u}) \\ \dot{\rho}_4 \mathbf{s}_4 + \rho_4 (\boldsymbol{\omega}_4 \times \mathbf{s}_4) &= \dot{\mathbf{p}} - \dot{c}_2 \mathbf{v} - c_2 (\boldsymbol{\omega}_p \times \mathbf{v}) \end{aligned} \tag{11}$$

where $\boldsymbol{\omega}_i$ stands for the angular velocity of the ith limb and $\boldsymbol{\omega}_p$ for the angular velocity of the mobile platform.

In order to cancel passive coordinates of Eq. (11), each of its equations can be dot-multiplied by its corresponding $\mathbf{s}_i$. Using the time derivative of Eqs. (3) and (4), operating, and simplifying, it yields

$$\begin{aligned} \dot{\rho}_1 &= \mathbf{s}_1 \cdot \dot{\mathbf{p}} + c_1 (\mathbf{u} \times \mathbf{s}_1) \cdot \boldsymbol{\omega}_P + K_1 \dot{\gamma}\ \mathbf{s}_1 \cdot \mathbf{u} \\ \dot{\rho}_2 &= \mathbf{s}_2 \cdot \dot{\mathbf{p}} + c_2 (\mathbf{v} \times \mathbf{s}_2) \cdot \boldsymbol{\omega}_P + K_2 \dot{\gamma}\ \mathbf{s}_2 \cdot \mathbf{v} \\ \dot{\rho}_3 &= \mathbf{s}_3 \cdot \dot{\mathbf{p}} - c_1 (\mathbf{u} \times \mathbf{s}_3) \cdot \boldsymbol{\omega}_P - K_1 \dot{\gamma}\ \mathbf{s}_3 \cdot \mathbf{u} \\ \dot{\rho}_4 &= \mathbf{s}_4 \cdot \dot{\mathbf{p}} - c_2 (\mathbf{v} \times \mathbf{s}_4) \cdot \boldsymbol{\omega}_P - K_2 \dot{\gamma}\ \mathbf{s}_4 \cdot \mathbf{v} \end{aligned} \tag{12}$$

where

$$\begin{aligned} K_1 &= \frac{-\cos\gamma\,(L/2 - e)}{\sin^2\gamma} \\ K_2 &= \frac{\cos\gamma\,(L/2 - e)^2}{\sin^3\gamma \quad r^2 - \dfrac{(L/2 - e)^2}{\sin^2\gamma}\Bigg)^{1/2}} \end{aligned} \tag{13}$$

Regarding Eq. (13), the value of term K_1 tends to be infinite when angle γ approaches zero. However, this does not happen if $e < L/2$. In turn, the denominator of K_2 is canceled or imaginary when

$$r^2 \leq \frac{\left(\dfrac{L}{2} - e\right)^2}{\sin^2\gamma} \tag{14}$$

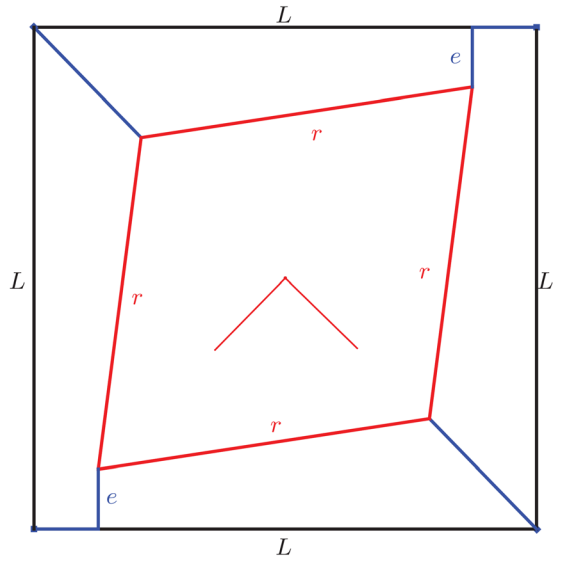

Fig. 7 Definition of *L*, *e*, and *r* from the top view of the mechanism

If the value of γ is such that Eq. (14) satisfies the equality, the value of K_2 and the Jacobian are not defined. In this case, the mechanism turns into a configuration in which the four bars of the articulated mobile platform are aligned, with $c_1 = r$ and $c_2 = 0$. This fact will be analyzed in Sec. 4.

From Eq. (12), the usual velocity equation in the form $\mathbf{J}_x\dot{\mathbf{x}} = \mathbf{J}_\rho\dot{\boldsymbol{\rho}}$ can be obtained, and $\dot{\mathbf{x}} = (\dot{x}_P, \dot{z}_P, \dot{\varphi}, \dot{\gamma})^{\mathrm{T}}$ and $\dot{\boldsymbol{\rho}} = (\dot{\rho}_1, \dot{\rho}_2, \dot{\rho}_3, \dot{\rho}_4)^{\mathrm{T}}$ being output and input velocity vectors, respectively. In order to obtain such an expression, mobile platforms linear and angular velocity vectors must be analyzed. Since the mobile platform has 4DOFs, components of $\dot{\mathbf{p}}$ and $\boldsymbol{\omega}_P$ in the fixed frame are

$$\begin{aligned} \dot{\mathbf{p}} &= \dot{x}_P\,\mathbf{i} + \dot{z}_P\,\mathbf{k} \\ \boldsymbol{\omega}_P &= \dot{\varphi}\,\mathbf{j} + \dot{\gamma}\,\mathbf{w} \end{aligned} \tag{15}$$

where $\mathbf{i}$, $\mathbf{j}$, and $\mathbf{k}$ are unit vectors in the x, y, and z directions, respectively.

If Eq. (15) is substituted in Eq. (12), we obtain

$$\begin{aligned} \dot{\rho}_1 &= \mathbf{s}_1 \cdot (\dot{x}_P\mathbf{i} + \dot{z}_P\mathbf{k}) + c_1(\mathbf{u} \times \mathbf{s}_1) \cdot (\dot{\varphi}\,\mathbf{j} + \dot{\gamma}\,\mathbf{w}) + K_1\,\dot{\gamma}\;\mathbf{s}_1 \cdot \mathbf{u} \\ \dot{\rho}_2 &= \mathbf{s}_2 \cdot (\dot{x}_P\mathbf{i} + \dot{z}_P\mathbf{k}) + c_2(\mathbf{v} \times \mathbf{s}_2) \cdot (\dot{\varphi}\,\mathbf{j} + \dot{\gamma}\,\mathbf{w}) + K_2\,\dot{\gamma}\;\mathbf{s}_2 \cdot \mathbf{v} \\ \dot{\rho}_3 &= \mathbf{s}_3 \cdot (\dot{x}_P\mathbf{i} + \dot{z}_P\mathbf{k}) - c_1(\mathbf{u} \times \mathbf{s}_3) \cdot (\dot{\varphi}\,\mathbf{j} + \dot{\gamma}\,\mathbf{w}) - K_1\,\dot{\gamma}\;\mathbf{s}_3 \cdot \mathbf{u} \\ \dot{\rho}_4 &= \mathbf{s}_4 \cdot (\dot{x}_P\mathbf{i} + \dot{z}_P\mathbf{k}) - c_2(\mathbf{v} \times \mathbf{s}_4) \cdot (\dot{\varphi}\,\mathbf{j} + \dot{\gamma}\,\mathbf{w}) - K_2\,\dot{\gamma}\;\mathbf{s}_4 \cdot \mathbf{v} \end{aligned} \tag{16}$$

From Eq. (16), the direct Jacobian $\mathbf{J}_x$ can be obtained, with inverse Jacobian $\mathbf{J}_\rho$ being the identity matrix

$$\mathbf{J}_x = \begin{bmatrix} \mathbf{s}_1 \cdot \mathbf{i} & \mathbf{s}_1 \cdot \mathbf{k} & c_1(\mathbf{u} \times \mathbf{s}_1) \cdot \mathbf{j} & c_1(\mathbf{u} \times \mathbf{s}_1) \cdot \mathbf{w} + K_1\,\mathbf{s}_1 \cdot \mathbf{u} \\ \mathbf{s}_2 \cdot \mathbf{i} & \mathbf{s}_2 \cdot \mathbf{k} & c_2(\mathbf{v} \times \mathbf{s}_2) \cdot \mathbf{j} & c_2(\mathbf{v} \times \mathbf{s}_2) \cdot \mathbf{w} + K_2\,\mathbf{s}_2 \cdot \mathbf{v} \\ \mathbf{s}_3 \cdot \mathbf{i} & \mathbf{s}_3 \cdot \mathbf{k} & -c_1(\mathbf{u} \times \mathbf{s}_3) \cdot \mathbf{j} & -c_1(\mathbf{u} \times \mathbf{s}_3) \cdot \mathbf{w} - K_1\,\mathbf{s}_3 \cdot \mathbf{u} \\ \mathbf{s}_4 \cdot \mathbf{i} & \mathbf{s}_4 \cdot \mathbf{k} & -c_2(\mathbf{v} \times \mathbf{s}_4) \cdot \mathbf{j} & -c_2(\mathbf{v} \times \mathbf{s}_4) \cdot \mathbf{w} - K_2\,\mathbf{s}_4 \cdot \mathbf{v} \end{bmatrix} \tag{17}$$

Using Jacobian matrix calculated in Eq. (17), actuator velocities for desired output velocities can be calculated as

$$\dot{\boldsymbol{\rho}} = \mathbf{J}_x\,\dot{\mathbf{x}} \tag{18}$$

4 Singularity Analysis

Singularities can be defined as configurations in which Jacobian matrices become singular [34]. They are usually considered as undesirable configurations of the mechanism in which the mobile platform can gain or lose instantaneous DOFs [1] and they can be avoided by actuation redundancy [35,36]. Such consideration is commonly referred to direct singularities in which the instantaneously gained DOFs may produce control problems and very high loads at the actuators. In Ref. [37], instead, it is shown how inverse singularities can be used in order to obtain better stiffness conditions.

In addition to direct and inverse kinematics, another type of singularities is architecture singularities, which can occur for specific values of geometric parameters of parallel robots, that fortunately can be avoided in early design stage [38]. Furthermore, an overall 6×6 Jacobian matrix for limited-DOF parallel manipulators is presented in Ref. [39], which can be divided into *Jacobian of constraints* and *Jacobian of actuations*, each of them having its specific singularities.

In this section, a singularity analysis of the proposed mechanism is carried out. Since the inverse Jacobian is the identity matrix, singularities are calculated based on the direct Jacobian matrix of Eq. (17). Additionally, an inverse singularity is also presented, which occurs when the denominator of K_2 of Eq. (13) vanishes.

Direct singularities occur when $\mathbf{J}_x$ becomes singular. In such cases, there is at least one direction in which the mechanism can move with blocked actuators. Such directions are given by the null space of $\mathbf{J}_x$. The null space of a $n \times n$ matrix—let us call it $\mathbf{A}$—is a subspace $\mathbf{R}^n$ whose vectors are perpendicular to any row of the said matrix. It can be expressed mathematically as

$$\mathbf{v}^* \in null(\mathbf{A}) \Longleftrightarrow \mathbf{A}\,\mathbf{v}^* = \mathbf{0} \tag{19}$$

Singularities of the direct Jacobian $\mathbf{J}_x$ of Eq. (17) are listed below together with their corresponding null space, which has been calculated with the MATLAB Symbolic Math Toolbox.

(1) $\mathbf{s}_i \perp \mathbf{i}, \forall i$. In this configuration, actuators 1 and 3 must be vertical with $\phi_1 = \phi_3 = \pi/2$. Additionally, actuators 2 and 4 must lie in the vertical y–z planes, with ψ_2 and ψ_4 being null. Then, the null space of the direct Jacobian is

$$\mathrm{null}(\mathbf{J}_x) = \begin{bmatrix} 1 \\ 0 \\ 0 \\ 0 \end{bmatrix} \tag{20}$$

Such null space shows that the mobile platform can move in the direction of coordinate x_P, that is, in the $\mathbf{i}$ direction. In this configuration, the mechanism instantaneously becomes a parallelogram in the x-z plane. However, the null space has been calculated regardless of the closed-loop equations of the mechanisms. A further analysis shows that this singular configuration is only possible for specific values of geometrical parameters. Specifically, for fixed L and e, length r must be defined as

$$r = \frac{L^2 - 2\,L\,e + 2\,e^2}{L - 2\,e} \tag{21}$$

Moreover, if such value of r and conditions derived from closed-loop equations are imposed, the null space of $\mathbf{J}_x$ can be recalculated resulting in a two-dimensional space

$$\mathrm{null}(\mathbf{J}_x) = \begin{bmatrix} 1 & 0 \\ 0 & 0 \\ 0 & 0 \\ 0 & 1 \end{bmatrix} \tag{22}$$

The resulting configuration has two instantaneous DOFs with fixed actuators: translation in the x direction and rotation around w. Figure 8 shows the mechanism in such configuration. Anyway, this singular configuration can be avoided by choosing geometrical parameters that does not verify Eq. (21).

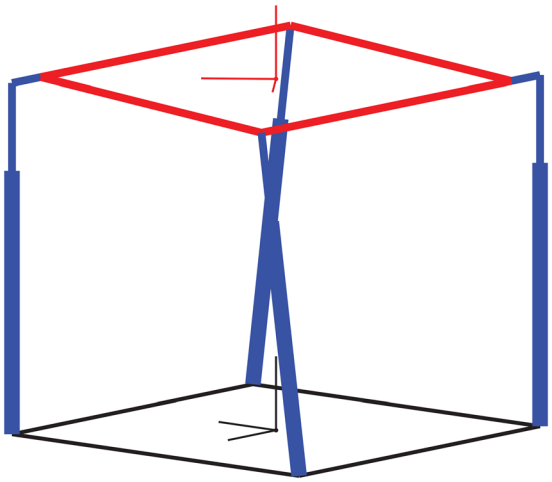

Fig. 8 Singular configuration with $\mathbf{s}_i \perp \mathbf{i}, \forall i$

(2) $\mathbf{s}_i \perp \mathbf{k}, \forall i$. All the prismatic actuators are in the $z=0$ horizontal plane with $\phi_1=\phi_2=\phi_3=\phi_4=0$. The null space of the direct Jacobian in such configuration is

$$\text{null}(\mathbf{J}_x) = \begin{bmatrix} 0 & 0 \\ 1 & 0 \\ 0 & 1 \\ 0 & 0 \end{bmatrix} \tag{23}$$

Now the mobile platform has two instantaneous DOFs with blocked actuators. On the one hand, it can move in the direction of the second coordinate z_P, that is, in the $\mathbf{k}$ direction; on the other hand, the third coordinate φ is also unlocked and the mobile platform can rotate around the $\mathbf{j}$ direction. In this configuration, the whole mechanism is contained in the $z=0$ plane, as shown in Fig. 9. Although direct singularities must be avoided, this configuration, or a configuration close to it, can be used in order to fold up the mechanism for its transportation.

(3) $\mathbf{s}_i \parallel \mathbf{u}, i=1,3$ and $\mathbf{s}_i \parallel \mathbf{v}, i=2,4$. This way, the third column of $\mathbf{J}_x$ (Eq. (17)) is canceled. The null space of $\mathbf{J}_x$ is

$$\text{null}(\mathbf{J}_x) = \begin{bmatrix} \sin\varphi \\ \cos\varphi \\ 0 \\ 0 \end{bmatrix} \tag{24}$$

In such configuration, the mechanism can move in the w direction, that is, a direction perpendicular to the mobile platform. For this singularity to happen, a geometric constraint is needed: length e of bars B_iC_i must be equal to $L/2$ in such a way that points C_1 and C_3 lie in the same vertical plane of P. Otherwise, vectors $\mathbf{s}_1$ and $\mathbf{s}_3$ cannot be perpendicular to $\mathbf{u}$. If $e=L/2$ geometric constraint is imposed, points C_1 and C_3 are restricted to move within the $y=0$ vertical plane. Moreover, if $e=L/2$ is fulfilled, the singularity will occur if $\mathbf{s}_i \parallel \mathbf{u}, i=1,3$, with $\mathbf{s}_i \parallel \mathbf{v}, i=2,4$, being not necessary to happen. However, for $\mathbf{s}_1$, $\mathbf{s}_3$, and $\mathbf{u}$ to be parallel, actuators 1 and 3 must lie in the same plane of the mobile platform. This fact is only possible in configurations

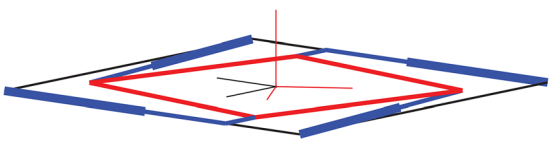

Fig. 9 Singular configuration with horizontal actuators

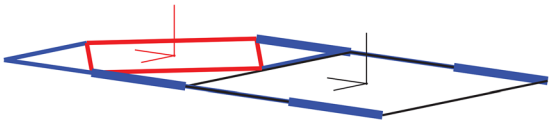

Fig. 10 Singular configuration with $\mathbf{s}_1 \parallel \mathbf{s}_3 \parallel \mathbf{u}$

in which the mobile platform is in the $z=0$ plane. Figure 10 shows the mechanism with the said geometric constraint in such type of singularity.In addition, fulfilling $e=L/2$ has another consequence: the mechanism cannot rotate around $\mathbf{w}$, losing one of its four output DOFs. This geometric constraint must be avoided if the mechanism must be used as a 4DOF rehabilitation robot. Nevertheless, if the rigid mobile platform, the guides and the slider are eliminated, coordinates c_1 or c_2 can be used as output DOF and the mechanism can be used for pick-and-place applications using the articulated mobile platform as a gripper.

(4) $\mathbf{s}_i = \mathbf{s}_j, \forall i,j$. All the prismatic actuators are parallel. In this case, the first two columns of $\mathbf{J}_x$ (Eq. (17)) are proportional. Then, the null space of $\mathbf{J}_x$ is

$$\text{null}(\mathbf{J}_x) = \begin{bmatrix} \sin\phi_1 \\ \cos\phi_1 \\ 0 \\ 0 \end{bmatrix} \tag{25}$$

The null space shows that the mobile platform can move perpendicular to the actuators, since all of them are parallel and inclined with angle ϕ_1. This is only possible if geometric parameters fulfill $e=0$ and $r=L$. If so, the mechanism instantaneously becomes a parallelogram. Figure 11 shows the mechanism in this type of configuration.

(5) Intersection of the directions of actuators 4 and 2 with actuators 1 and 3, respectively. This is a common singularity in mechanisms with prismatic actuators like the Gough–Stewart platform [40]. In such configuration, the null space of $\mathbf{J}_x$ is

$$\text{null}(\mathbf{J}_x) = \begin{bmatrix} z_P - \dfrac{L\,\sin\phi_1 \sin\phi_3}{\sin(\phi_1+\phi_3)} \\ \dfrac{L\,\sin(\phi_1-\phi_3)}{2\,\sin(\phi_1+\phi_3)} - x_P \\ 1 \\ 0 \end{bmatrix} \tag{26}$$

In this type of singular configuration, bars C_1C_4 and C_3C_2 are aligned with bars B_1C_1 and B_3C_3, respectively. The null space of $\mathbf{J}_x$ shows that the mobile platform does not rotate around $\mathbf{w}$, so the articulated mobile platform behaves like a rigid body. Then, with blocked actuators, the mechanism becomes a four-bar linkage in the x–z plane and the *instantaneously rigid* mobile platform can rotate around

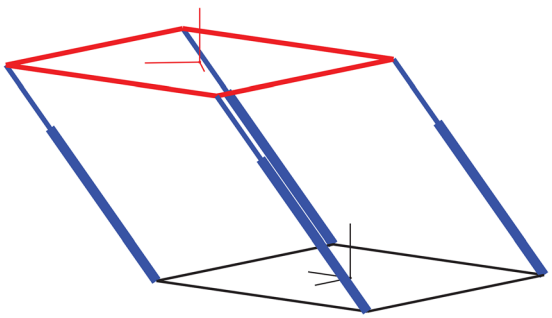

Fig. 11 Singular configuration with parallel actuators

its *instantaneous screw axis* with respect to the ground. Figure 12 shows the mechanism in such configuration and Fig. 13 shows the same configuration with the prolongation of the actuators direction until the intersection. Each pair of crossing lines in Fig. 13(*a*) defines a plane. The intersection of these planes defines the *instantaneous screw axis* of the *instantaneously rigid* mobile platform with respect to the ground. Figure 13(*b*) shows how the said planes are crossed.

(6) $c_2 = 0$ or $c_1 = 0$. The four bars of the articulated mobile platform lie in a line. If $e \neq L/2$, which is necessary to avoid one of the previous singularities, $c_1 = 0$ is not possible and only $c_2 = 0$ can happen when points C_2 and C_4 coincide. For c_2 to be zero, the value of γ must be the one that holds the equality in Eq. (14). As explained before, the defined coordinates c_1 and c_2 describe the movement of points (C_1, C_3) and (C_2, C_4), respectively, with opposite sign. Hence, when coordinate c_2 increases from $c_2 = 0$, it is not possible that points C_2 and C_4 continue in superposition, they take separate ways. In fact, this is an inverse singularity since the said value of γ is a limit of the range of the coordinate. Therefore, the calculation of the null space of $\mathbf{J}_x$ makes no sense here. A configuration of this type is shown in Fig. 14. Nevertheless, the physical interaction of the parts of the mechanism avoids this kind of singularities, as can be seen in Fig. 4 in which the guides avoid the physical superposition of the sliders.

(7) By numerical analysis, another singularity can be found which, in general, does not satisfy apparent geometric conditions. An expression of its nullspace can be written as follows:

$$\text{null}(\mathbf{J}_x) = \begin{bmatrix} R_2\,S_1\,s\phi_3 - R_1\,S_2\,s\phi_3 - R_2\,S_3\,s\phi_1 + R_3\,S_2\,s\phi_1 + R_1\,S_3\,c\psi_2\,s\phi_2 - R_3\,S_1\,c\psi_2\,s\phi_2 \\ R_1\,S_2\,c\phi_3 - R_2\,S_1\,c\phi_3 - R_2\,S_3\,c\phi_1 + R_3\,S_2\,c\phi_1 - R_1\,S_3\,s\psi_2 + R_3\,S_1\,s\psi_2 \\ S_3\,s\phi_1\,s\psi_2 - S_2\,c\phi_3\,s\phi_1 - S_1\,s\phi_3\,s\psi_2 - S_2\,c\phi_1\,s\phi_3 + S_1\,c\phi_3\,c\psi_2\,s\phi_2 + S_3\,c\phi_1\,c\psi_2\,s\phi_2 \\ R_2\,c\phi_1\,s\phi_3 + R_2\,c\phi_3\,s\phi_1 + R_1\,s\phi_3\,s\psi_2 - R_3\,s\phi_1\,s\psi_2 - R_1\,c\phi_3\,c\psi_2\,s\phi_2 - R_3\,c\phi_1\,c\psi_2\,s\phi_2 \end{bmatrix} \tag{27}$$

where s and c stand, respectively, for sin and cos and

$$R_1 = \frac{\text{Le}\,c\gamma\,c\phi_1\,s\varphi}{s\gamma} - \frac{\text{Le}\,c\gamma\,c\varphi\,s\phi_1}{s\gamma}$$

$$R_2 = c_2\,s\gamma\,s\psi_2\,s\varphi + c_2\,c\psi_2\,c\varphi\,s\gamma\,s\phi_2$$

$$R_3 = \frac{\text{Le}\,c\gamma\,c\phi_3\,s\varphi}{s\gamma} + \frac{\text{Le}\,c\gamma\,c\varphi\,s\phi_3}{s\gamma}$$

$$S_1 = c\phi_1 \quad \text{Le}\,c\varphi + \frac{\text{Le}\,c^2\gamma\,c\varphi}{s^2\gamma}\Bigg) + s\phi_1 \quad \text{Le}\,s\varphi + \frac{\text{Le}\,c^2\gamma\,s\varphi}{s^2\gamma}\Bigg)$$

$$S_2 = \frac{r^2\,c\gamma\,c\psi_2\,s\phi_2\,s\varphi}{c_2} - \frac{c\phi_2\,c\psi_2\left(r^2\,c^2\gamma - c_2{}^2\right)}{c_2\,s\gamma} - \frac{r^2\,c\gamma\,c\varphi\,s\psi_2}{c_2}$$

$$S_3 = c\phi_3 \quad \text{Le}\,c\varphi + \frac{\text{Le}\,c^2\gamma\,c\varphi}{s^2\gamma}\Bigg) - s\phi_3 \quad \text{Le}\,s\varphi + \frac{\text{Le}\,c^2\gamma\,s\varphi}{s^2\gamma}\Bigg)$$

$$\text{Le} = \frac{L}{2} - e$$

Although this type of singularity does not have an apparent geometric identity, there are particular cases for which some geometric conditions are fulfilled:

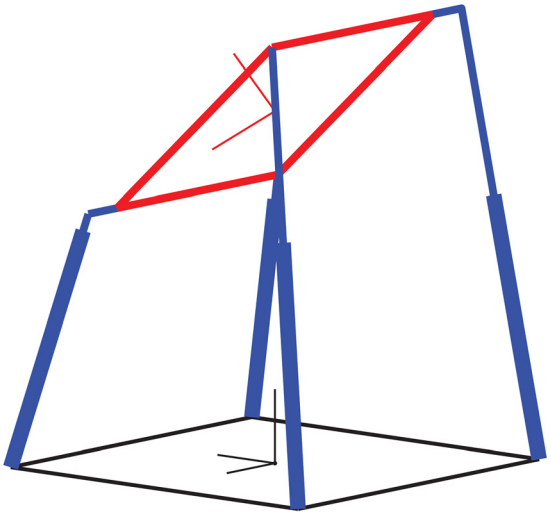

Fig. 12 Singular configuration with intersection of actuators directions (I)

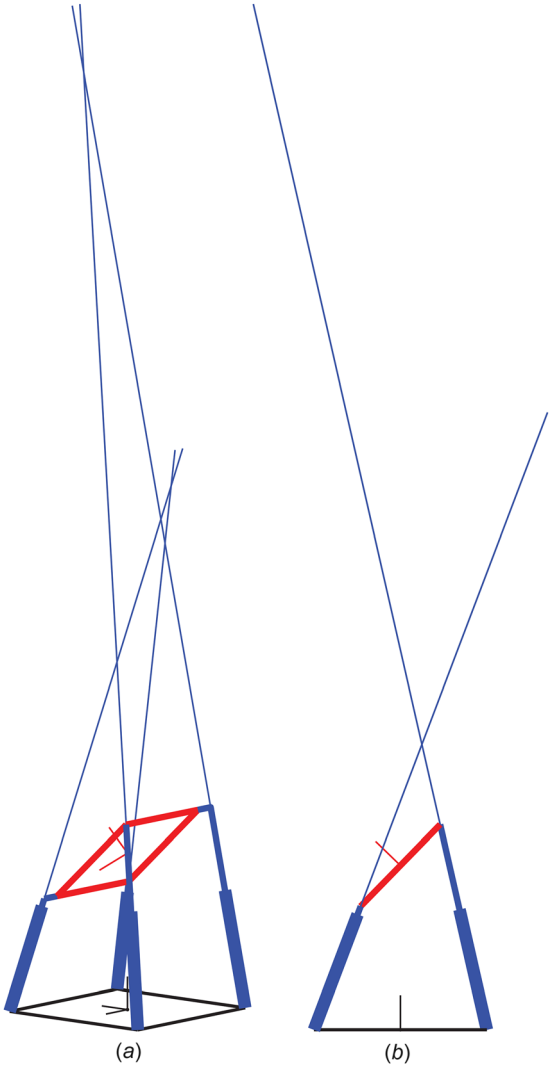

Fig. 13 Singular configuration with intersection of actuators directions (II): (*a*) isometric view and (*b*) front view

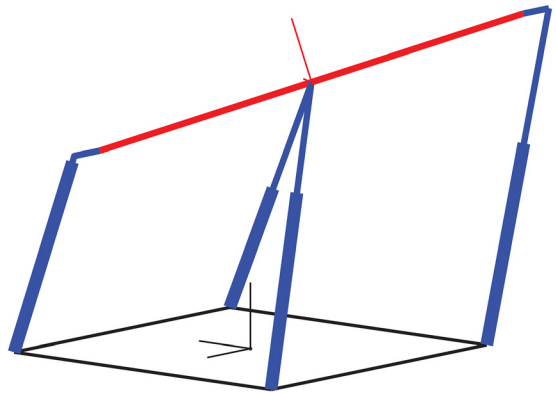

Fig. 14 Singular configuration with $c_2 = 0$

- $x_P = 0$ and $\varphi \neq 0$. In this case, actuators 2 and 4 lie in the vertical parallel planes. Figure 15 shows the mechanism in this configuration. Two vertical planes containing actuators 2 and 4 are also represented.
- $x_P \neq 0$ and $\varphi = 0$. This time the singularity appears for two specific values of γ, which do not change for any values of x_P and z_P. Specifically, the singularities occur at $\gamma \approx 1.248$ rad and $\gamma \approx 1.986$ rad. Then, it gives an interesting range of γ free of singularities of around 0.738 rad (42 deg) for $\varphi = 0$.
- $x_P = 0$ and $\varphi = 0$. It is a particular case of the previous ones for which the nullspace of Eq. (27) becomes the simple expression shown in the following equation:

$$\text{null}(\mathbf{J}_x) = \begin{bmatrix} 0 \\ -\left(\dfrac{L}{2} - e\right) \\ \hline \tan\phi_1 \sin^2\gamma \\ 0 \\ 1 \end{bmatrix} \tag{28}$$

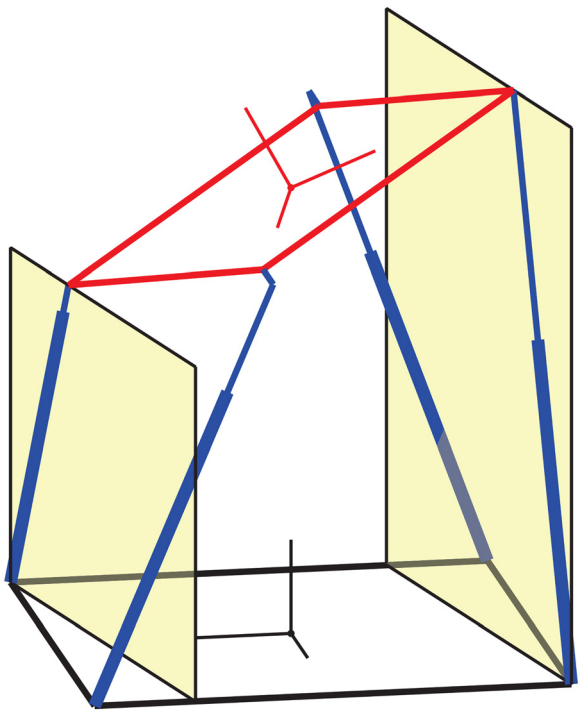

Fig. 15 Singular configuration with actuators 2 and 4 in vertical parallel planes

Notice that the nullspace of Eq. (28) shows an instantaneous screw motion about the axis perpendicular to the mobile platform.

Most singularities described earlier should be avoided. The only exception is the second one, which will be useful for folding up the mechanism and, fortunately, it will be far from the trajectories of rehabilitation maneuvers. The other types of singularities can be harmful, but most of them can be avoided by choosing appropriate values for the geometric parameters L, r, and e. The fifth and the seventh ones are the only harmful singularities, which can appear for any set of values of the geometric parameters. Section 5 analyzes the location of these singularities within the workspace in order to find a singularity-free domain in which rehabilitation maneuvers can be carried out.

5 Location of the Singularities in the Workspace

In Sec. 4, the possible singularities of the 2RPRR-2 UPS mechanism have been described. Although most of them can be avoided with suitable values of the geometric parameters of the mechanism, this is not the case of the second and the seventh types of singularities. Then, it is necessary to know the location of these singularities within the workspace. Nevertheless, since the mechanism has four DOFs, the graphical representation of such singularity locus is not possible. This issue is usually overcome by analyzing a constant orientation or translational workspace and orientation workspace for a fixed position [41–43]. Such separation will be used here.

The geometry of the robot is defined by three parameters, namely, the length L of the side of the fixed base, the length e of bars B_1C_1 and B_3C_3, and the length r of the four identical bars of the articulated mobile platform. Numeric values of this parameters are shown in Table 1, together with the strokes of the prismatic actuators.

Before analyzing the singularities, an observation must be done concerning the workspace of the mechanism. Since it has prismatic actuators, the workspace is limited mainly by their strokes. In fact, this is the only limitation for coordinates x_P, z_P, and φ. The range of coordinate γ, in turn, is limited by the values of the geometric parameters of the mechanism. Hence, the workspace of γ will be analyzed first, followed by the orientation workspace and translation one. Finally, a rehabilitation maneuver will be described.

5.1 Workspace of γ. In order to look for the values of γ for which the fifth and sixth type singularities occur, a representation of the platform in its own plane is very helpful. In Fig. 16, the platform is drawn in its own plane in both singular configurations. In order to make the figure clearer, actuators A_1B_1, A_2C_2, A_3B_3, and A_4C_4 have been omitted.

The sixth type singularities (the one represented and its symmetric with respect to the y-axis) determine the limits of the workspace of γ. From trigonometrical inspection of Fig. 16, limit $\gamma_{\min}$ of the workspace of γ can be calculated. Because of the symmetry, $\gamma_{\max}$ can be also calculated

$$\gamma^6_{\min} = a\sin\left(\frac{L/2 - e}{r}\right), \quad \gamma^6_{\max} = \pi - \gamma^6_{\min} \tag{29}$$

On the other hand, the fifth type singularity divides the workspace into two sets. Bearing in mind that in the fifth singularity

Table 1 Geometric parameters and strokes of actuators

L (m)	e (m)	r (m)	$\rho_{\min}$ (m)	$\rho_{\max}$ (m)
0.42	0.05	0.28	0.4	0.75

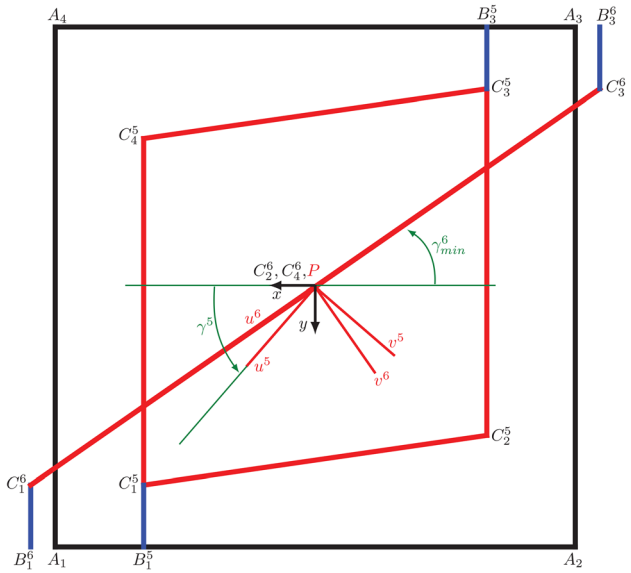

Fig. 16 Platform in the fifth and sixth singularity configurations

bars B_1C_1 and C_1C_4 are aligned, the value of γ in this singularity is

$$\gamma^5 = a\sin\left(\sqrt{\frac{L/2-e}{r}}\right) \tag{30}$$

Evaluating γ^5, $\gamma^6_{\min}$, and $\gamma^6_{\max}$ for the possible values of $((L/2-e)/r)$, Fig. 17 shows how the fifth type singularity divides the workspace into two different regions. As the bright region provides the largest ranges for γ, small values of $(L/2-e/r)$ are preferred in order to maximize it. For the values of L, e, and r selected in this paper, the ranges of motion for γ are from 0.6082 to 2.533 rad shown by the vertical line of Fig. 17. The singularity of fifth type will occur at $\gamma = 0.8571$ rad and the other type singularities may occur between $\gamma^6_{\min}$ and $\gamma^6_{\max}$, as will be shown next.

5.2 Orientation Workspace. The orientation workspace is calculated by fixing the value of coordinates x_P and z_P and calculating the range of motion for angular coordinates φ and γ. The way to create such a workspace is making a mesh with numeric values of coordinates φ and γ and, if the location is reachable with the strokes of the actuators, calculating the condition number of $\mathbf{J}_x$.

Taking into account the requirements of a rehabilitation task and the results of Sec. 5.1 for γ, the considered ranges of motion for φ and γ are from $-\pi/2$ to $\pi/2$ radians and from $\gamma^6_{\min}$ to $\gamma^6_{\max}$, respectively. The orientation workspace is calculated for the sets of values $[x_P = 0\ m,\ z_P = 0.55\ m]$ and $[x_P = 0.2\ m,\ z_P = 0.55\ m]$ of the Cartesian coordinates. Results are shown in Fig. 18 in which the yellow colored lines show the locations in which $\mathbf{J}_x$ is ill-conditioned. The results for negative values of x_P are not calculated since they will be symmetric to the positive ones due to the symmetry of the mechanism.

From Fig. 18, it can be seen that for a fixed value of γ, namely $\gamma = 0.8571\ i$, there is a yellow, straight vertical line. This is the singularity of the fifth type described in Sec. 4 whose location does not depend on the values of the other coordinates. It happens for the said specific value of γ when bar C_1C_4 is aligned with bar B_1C_1. On the other hand, the other two yellow curves are dependent on the values of the coordinates. Both are singularities of the seventh type presented in Sec. 4. Although their location changes slightly, there is portion of the workspace free of singularities between these two curves which can be used for rehabilitation tasks. There, the range of motion of φ and γ is ± 0.6 rad (± 30 deg) and [1.4 rad, 1.9 rad] (~ 28 deg), respectively. These ranges

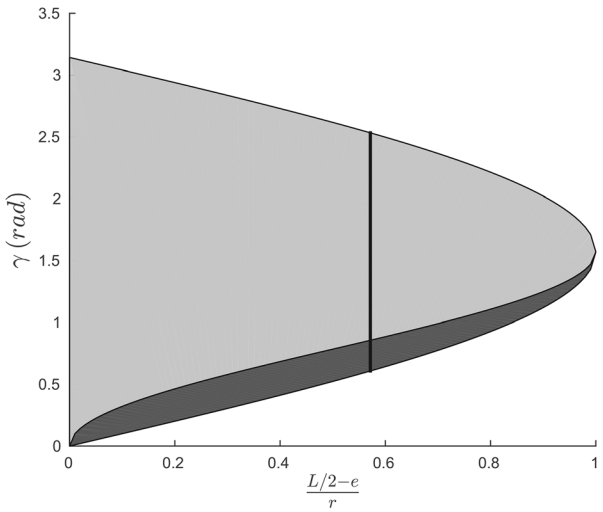

Fig. 17 Workspace of γ in terms of $((L/2-e)/r)$

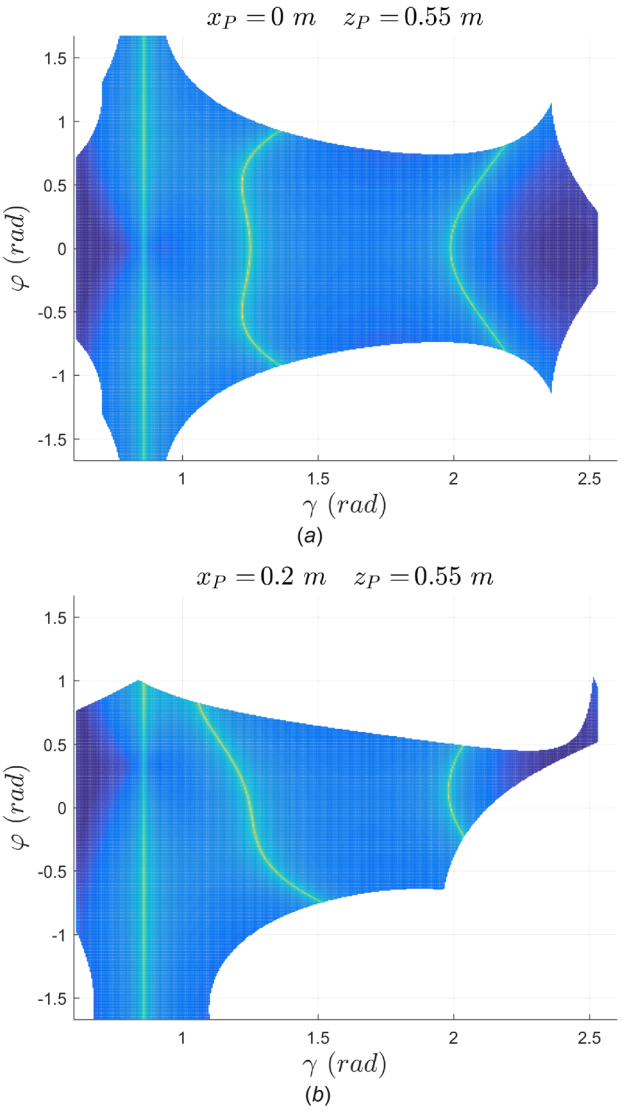

Fig. 18 Singularities in the orientation workspace: (*a*) $x_p = 0$ m, $z_p = 0.55$ m and (*b*) $x_p = 0.2$ m, $z_p = 0.55$ m

of motion will be validated and completed analyzing the translation workspace.

5.3 Translation Workspace. A translation or constant orientation workspace can be represented by fixing values of coordinates φ and γ and evaluating the reachable values of x_P and z_P and the condition number of $\mathbf{J}_x$ when possible. In order to avoid the second singularity, which as said before can be used to fold up the mechanism, values of z_P start from 0.05 meters. From the results of Sec. 5.2, it is expected that for values of $x_P \in [-0.2\ m, 0.2\ m]$ and $z_P = 0.55\ m$ with orientations defined by values of $\varphi \in [-0.6, 0.6]$ and $\gamma \in [1.4, 1.9]$, there will be no singularities. This premise is accomplished in Fig. 19 in which the translation workspace is shown for the values $[\varphi = 0\,\text{rad},\ \gamma = 1.65\,\text{rad}]$ and $[\varphi = 0.5\,\text{rad},\ \gamma = 1.65\,\text{rad}]$ of the angular coordinates. Notice that the absence of yellow lines means that the condition number of $\mathbf{J}_x$ is approximately constant and, consequently, there are no singularities for the used angles.

Taking into account the results of Figs. 18 and 19, Table 2 shows a range of values of the output coordinates which is free of singularities and wide enough to perform the rehabilitation maneuver shown next.

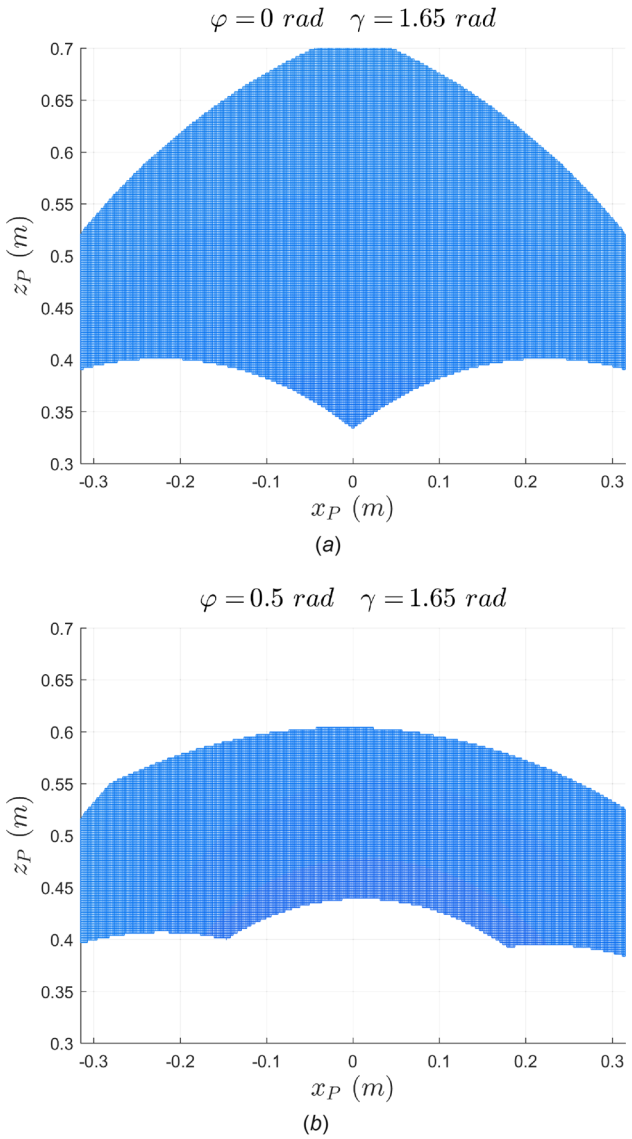

Fig. 19 Lack of singularities in the translation workspace: (*a*) $\varphi = 0$ rad, $\gamma = 1.65$ rad and (*b*) $\varphi = 0.5$ rad, $\gamma = 1.65$ rad

Table 2 Singularity-free ranges of motion

Coord.	x_P (m)	z_P (m)	φ (rad)	γ (rad)
Min	–0.20	0.44	–0.60	1.5
Max	0.20	0.60	0.60	1.9

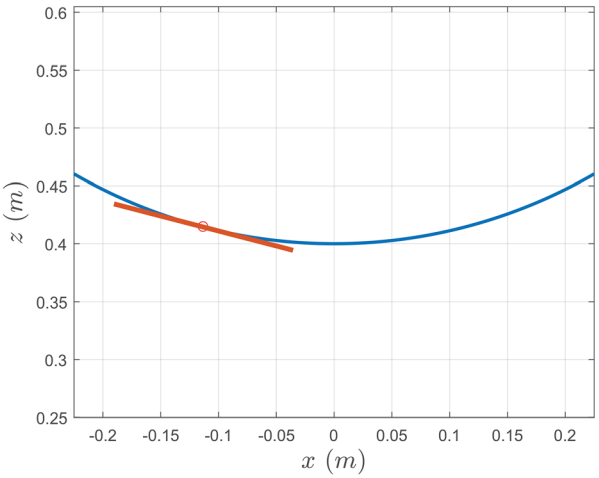

Fig. 20 Rehabilitation trajectory in the *x–z* plane

5.4 Analysis of a Rehabilitation Maneuver. Based on the Lanchman test, a rehabilitation trajectory can be defined as an arc of circumference of radius 0.45 m in the x–z tibiofemoral plane, for a constant value of γ and rotating the mobile platform in such a way that it is always tangent to the arc. Figure 20 shows this trajectory in the x–z plane with an instantaneous projection of the mobile platform.

The values of the input coordinates ρ_i along the trajectory are presented in Fig. 21 with respect to the trajectory values of x_P. Notice that the values of inputs ρ_i are within the stroke limits of the actuators.

This trajectory can be performed for any value of $\gamma \in [1.5, 1.9]$. The condition number of $\mathbf{J}_x$ shows that the rehabilitation maneuver can be carried out for the said values of γ in a singularity-free zone. As a result, a Pivot Shift test can be carried out at any point of the trajectory, varying the value of $\gamma \pm 0.2$ rad (± 11 deg).

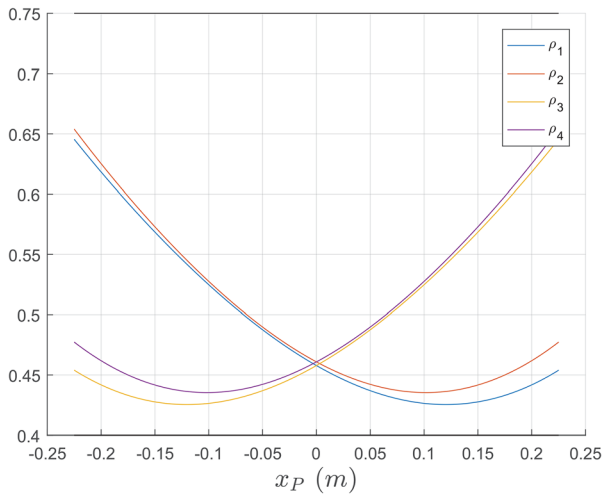

Fig. 21 Values of input coordinates ρ_i along the trajectory

6 Conclusions

A new 2T2R parallel mechanism has been designed for its application as a knee rehabilitation robot. The mechanism is able to carry out the needed movements for the Lanchman and pivot shift tests. The desired output movements are reached by means of an articulated mobile platform which allows large rotations in the tibiofemoral plane needed for the Lanchman test and small rotations around the an axis perpendicular to the mobile platform needed for the pivot shift test. Kinematics of the designed mechanism makes it a folding mechanism that occupies little volume when folded in order to be transported. This feature is achieved by taking the manipulator to a singularity or its neighborhood. Other singularities of the mechanism have been also analyzed and it has been shown how some of them can be avoided choosing suitable values for the geometric parameters of the mechanism. The location of the remaining singularities within the workspace has been analyzed and a portion of workspace free of singularities has been determined in which rehabilitation tasks can be carried out. Together with the singularity analysis, the null space of the direct Jacobian has been calculated in order to know how the mechanism would move with blocked actuators if each singularity was reached. Next steps of the design stage include the analysis of the workspace and the optimization of the mechanism in order to build a prototype.

Funding Data

- This work was funded by the Plan Nacional de I + D, Comisión Interministerial de Ciencia y Tecnología (FEDER-CICYT) under the projects DPI2013-44227-R and DPI2017-84201-R.

References

[1] Merlet, J., 2006, *Parallel Robots*, Springer, Dordrecht, The Netherlands.

[2] Neumann, K.-E., 1988, "Robot," Parallel Kinematics Machines SL, U.S. Patent No. 4732525A.

[3] Zhang, D., Bi, Z., and Li, B., 2009, "Design and Kinetostatic Analysis of a New Parallel Manipulator," Rob. Comput.-Integr. Manuf., **25**(4–5), pp. 782–791.

[4] Chablat, D., and Wenger, P., 2003, "Architecture Optimization of a 3-DOF Translational Parallel Mechanism for Machining Applications, the Orthoglide," IEEE Trans. Rob. Autom., **19**(3), pp. 403–410.

[5] Clavel, R., 1990, "Device for the Movement and Positioning of an Element in Space," U.S. Patent No. 4976582A.

[6] Salgado, O., Altuzarra, O., Petuya, V., and Hernández, A., 2008, "Synthesis and Design of a Novel 3T1R Fully-Parallel Manipulator," ASME J. Mech. Des., **130**(4), p. 042305.

[7] Briot, S., and Bonev, I. A., 2009, "Pantopteron: A New Fully Decoupled 3DOF Translational Parallel Robot for Pick-and-Place Applications," ASME J. Mech. Rob., **1**(2), p. 021001.

[8] Company, O., Pierrot, F., Krut, S., Baradat, C., and Nabat, V., 2011, "Par2: A Spatial Mechanism for Fast Planar Two-Degree-of-Freedom Pick-and-Place Applications," Meccanica, **46**(1), pp. 239–248.

[9] Xie, F., and Liu, X.-J., 2015, "Design and Development of a High-Speed and High-Rotation Robot With Four Identical Arms and a Single Platform," ASME J. Mech. Rob., **7**(4), p. 041015.

[10] Kuo, C.-H., and Dai, J. S., 2012, "Kinematics of a Fully-Decoupled Remote Center-of-Motion Parallel Manipulator for Minimally Invasive Surgery," ASME J. Med. Devices, **6**(2), p. 021008.

[11] Bi, Z. M., 2013, "Design of a Spherical Parallel Kinematic Machine for Ankle Rehabilitation," Adv. Rob., **27**(2), pp. 121–132.

[12] Chaker, A., Mlika, A., Laribi, M. A., Romdhane, L., and Zeghloul, S., 2012, "Synthesis of Spherical Parallel Manipulator for Dexterous Medical Task," Front. Mech. Eng., **7**(2), pp. 150–162.

[13] Plitea, N., Szilaghyi, A., and Pisla, D., 2015, "Kinematic Analysis of a New 5-DOF Modular Parallel Robot for Brachytherapy," Rob. Comput. Integr. Manuf., **31**, pp. 70–80.

[14] Jamwal, P. K., Hussain, S., and Xie, S. Q., 2015, "Review on Design and Control Aspects of Ankle Rehabilitation Robots," Disability Rehabilitation: Assistive Technol., **10**(2), pp. 93–101.

[15] Rastegarpanah, A., Saadat, M., and Borboni, A., 2016, "Parallel Robot for Lower Limb Rehabilitation Exercises," Appl. Bionics Biomech., **2016**, p. 8584735.

[16] Wiertsema, S., van Hooff, H., Migchelsen, L., and Steultjens, M., 2008, "Reliability of the KT1000 Arthrometer and the Lachman Test in Patients With an ACL Rupture," Knee, **15**(2), pp. 107–110.

[17] Lopomo, N., Zaffagnini, S., Signorelli, C., Bignozzi, S., Giordano, G., Muccioli, G. M. M., and Visani, A., 2012, "An Original Clinical Methodology for Non-Invasive Assessment of Pivot-Shift Test," Comput. Methods Biomech. Biomed. Eng., **15**(12), pp. 1323–1328.

[18] Andriacchi, T. P., Natarajan, R., and Hurwitz, D., 1997, "Musculoskeletal Dynamics: Locomotion and Clinical Applications," *Basic Orthopaedic Biomechanics & Mechanobiology*, Vol. 2, Lippincott Willians & Wikins, Philadelphia, PA, pp. 37–68.

[19] Chen, W., and Zhao, M., 2001, "A Novel 4-DOF Parallel Manipulator and Its Kinematic Modelling," IEEE International Conference on Robotics and Automation (ICRA), Seoul, South Korea, May 21–26, pp. 3350–3355.

[20] Fan, C., Liu, H., and Zhang, Y., 2013, "Type Synthesis of 2T2R, 1T2R and 2R Parallel Mechanisms," Mech. Mach. Theory, **61**, pp. 184–190.

[21] Ghaffari, H., Payeganeh, G., and Arbabtafti, M., 2014, "Kinematic Design of a Novel 4-DOF Parallel Mechanism for Turbine Blade Machining," Int. J. Adv. Manuf. Technol., **74**(5–8), pp. 729–739.

[22] Altuzarra, O., Macho, E., Aginaga, J., and Petuya, V., 2015, "Design of a Solar Tracking Parallel Mechanism With Low Energy Consumption," Proc. Inst. Mech. Eng., Part C, **229**(3), pp. 566–579.

[23] Gan, D., Dai, J. S., Dias, J., Umer, R., and Seneviratne, L., 2015, "Singularity-Free Workspace Aimed Optimal Design of a 2T2R Parallel Mechanism for Automated Fiber Placement," ASME J. Mech. Rob., **7**(4), p. 041022.

[24] Kumar, N., Piccin, O., and Bayle, B., 2014, "A Task-Based Type Synthesis of Novel 2T2R Parallel Mechanisms," Mech. Mach. Theory, **77**, pp. 59–72.

[25] Mohan, S., Mohanta, J., Kurtenbach, S., Paris, J., Corves, B., and Huesing, M., 2017, "Design, Development and Control of a 2PRP-2PPR Planar Parallel Manipulator for Lower Limb Rehabilitation Therapies," Mech. Mach. Theory, **112**, pp. 272–294.

[26] Ding, H., ao Cao, W., Chen, Z., and Kecskeméthy, A., 2015, "Structural Synthesis of Two-Layer and Two-Loop Spatial Mechanisms With Coupling Chains," Mech. Mach. Theory, **92**, pp. 289–313.

[27] Wang, C., Fang, Y., and Fang, H., 2017, "Novel 2R3T and 2R2T Parallel Mechanisms With High Rotational Capability," Robotica, **35**(2), pp. 401–418.

[28] Araujo-Gómez, P., Díaz-Rodríguez, M., Mata, V., Valera, A., and Page, A., 2016, "Design of a 3-UPS-RPU Parallel Robot for Knee Diagnosis and Rehabilitation," *ROMANSY 21—Robot Design, Dynamics and Control*, Vol. 569, CISM International Centre for Mechanical Sciences, Udine, Italy, pp. 303–310.

[29] Araujo-Gómez, P., Mata, V., Díaz-Rodríguez, M., Valera, A., and Page, A., 2017, "Design and Kinematic Analysis of a Novel 3 UPS/RPU Parallel Kinematic Mechanism With 2T2R Motion for Knee Diagnosis and Rehabilitation Tasks," ASME J. Mech. Rob., **9**(6), p. 061004.

[30] Nabat, V., de la, O., Rodríguez, M., Company, O. Krut, S., and Pierrot, V., 2005, "Par4: Very High Speed Parallel Robot for Pick-and-Place," IEEE/RSJ International Conference on Intelligent Robots and Systems (IROS), Edmonton, AB, Canada, Aug. 2–6, pp. 553–558.

[31] Lambert, P., and Herder, J. L., 2015, "A Novel Parallel Haptic Device With 7 Degrees of Freedom," IEEE World Haptics Conference (WHC), Evanston, IL, June 22–26, pp. 183–188.

[32] Hoevenaars, A., Gosselin, C., Lambert, P., and Herder, J., 2017, "A Systematic Approach for the Jacobian Analysis of Parallel Manipulators With Two End-Effectors," Mech. Mach. Theory, **109**, pp. 171–194.

[33] Song, Y., Qi, Y., and Sun, T., 2016, "Conceptual Design and Kinematic Analysis of a Novel Parallel Manipulator With an Articulated Gripping Platform," *Advances in Reconfigurable Mechanisms and Robots II* (Mechanism and Machine), X. Ding, X. Kong, and J. Dai, eds., Vol. 36, Springer International Publishing, Beijing, China, pp. 433–444.

[34] Gosselin, C., and Angeles, J., 1990, "Singularity Analysis of Closed-Loop Kinematic Chains," IEEE Trans. Rob. Autom., **6**(3), pp. 281–290.

[35] Wang, J., and Gosselin, C. M., 2004, "Kinematic Analysis and Design of Kinematically Redundant Parallel Mechanisms," ASME J. Mech. Des., **126**(1), pp. 109–118.

[36] Isaksson, M., 2017, "Kinematically Redundant Planar Parallel Mechanisms for Optimal Singularity Avoidance," ASME J. Mech. Des., **139**(4), p. 042302.

[37] Aginaga, J., Zabalza, I., Altuzarra, O., and Nájera, J., 2012, "Improving Static Stiffness of the 6-RUS Parallel Manipulator Using Inverse Singularities," Rob. Comput.-Integr. Manuf., **28**(4), pp. 458–471.

[38] Ma, O., and Angeles, J., 1991, "Architecture Singularities of Platform Manipulators," IEEE International Conference on Robotics and Automation (ICRA), Sacramento, CA, Apr. 9–11, pp. 1542–1547.

[39] Joshi, S. A., and Tsai, L.-W., 2002, "Jacobian Analysis of Limited-DOF Parallel Manipulators," ASME J. Mech. Des., **124**(2), pp. 254–258.

[40] St-Onge, B. M., and Gosselin, C. M., 2000, "Singularity Analysis and Representation of the General Gough-Stewart Platform," Int. J. Rob. Res., **19**(3), pp. 271–288.

[41] Merlet, J. P., 1999, "Determination of 6D Workspaces of Gough-Type Parallel Manipulator and Comparison Between Different Geometries," Int. J. Rob. Res., **18**(9), pp. 902–916.

[42] Bonev, I. A., and Ryu, J., 2001, "A Geometrical Method for Computing the Constant-Orientation Workspace of 6-PRRS Parallel Manipulators," Mech. Mach. Theory, **36**(1), pp. 1–13.

[43] Bonev, I. A., and Ryu, J., 2001, "A New Approach to Orientation Workspace Analysis of 6-DOF Parallel Manipulators," Mech. Mach. Theory, **36**(1), pp. 15–28.